

# Measurement of spin memory lengths in PdNi and PdFe ferromagnetic alloys

H. Arham, T. S. Khaire, R. Loloee, W. P. Pratt, Jr., and Norman O. Birge\*

*Department of Physics and Astronomy, Michigan State University, East Lansing, MI 48824-2320*

(Dated: November 2, 2018)

Weakly ferromagnetic alloys are being used by several groups in the study of superconducting/ferromagnetic hybrid systems. Because spin-flip and spin-orbit scattering in such alloys disrupt the penetration of pair correlations into the ferromagnetic material, it is desirable to have a direct measurement of the spin memory length in such alloys. We have measured the spin memory length at 4.2 K in sputtered Pd<sub>0.88</sub>Ni<sub>0.12</sub> and Pd<sub>0.987</sub>Fe<sub>0.013</sub> alloys using methods based on current-perpendicular-to-plane giant magnetoresistance. The alloys are incorporated into hybrid spin valves of various types, and the spin memory length is determined by fits of the Valet-Fert spin-transport equations to data of magnetoresistance vs. alloy thickness. For the case of PdNi alloy, the resulting values of the spin memory length are  $l_{sf}^{PdNi} = 2.8 \pm 0.5$  nm and  $5.4 \pm 0.6$  nm, depending on whether or not the PdNi is exchange biased by an adjacent Permalloy layer. For PdFe, the spin memory length is somewhat longer,  $l_{sf}^{PdFe} = 9.6 \pm 2$  nm, consistent with earlier measurements indicating lower spin-orbit scattering in that material. Unfortunately, even the longer spin memory length in PdFe may not be long enough to facilitate observation of spin-triplet superconducting correlations predicted to occur in superconducting/ferromagnetic hybrid systems in the presence of magnetic inhomogeneity.

PACS numbers: 74.50.+r, 73.23.-b, 85.25.Am, 85.25.Cp

The interplay between ferromagnetism and superconductivity has piqued the interest of physicists for several decades.<sup>1</sup> In hybrid superconducting/ferromagnetic (S/F) systems, the strong exchange field in the F material limits the penetration of superconducting pair correlations (the proximity effect) to very short distances, of order  $\xi_F = \sqrt{\hbar D/E_{ex}}$  in the dirty limit, where  $D$  and  $E_{ex}$  are the diffusion coefficient and exchange energy, respectively, in the F material.<sup>2</sup> Several groups studying S/F systems have used weakly ferromagnetic alloys to reduce  $E_{ex}$  and hence increase  $\xi_F$ .<sup>3,4</sup> Ryazanov and co-workers<sup>5</sup> fabricated S/F/S Josephson junctions using CuNi alloy as the F material, and found a very rapid decrease of the critical current with CuNi thickness, probably due to spin-flip scattering from small magnetic clusters in the inhomogeneous magnetic alloy.<sup>6</sup> Kontos *et al.*<sup>7</sup> found a somewhat slower decrease in critical current vs. thickness of S/I/F/S junctions with PdNi alloy as the F material, raising the hope that the spin memory length in PdNi might be considerably longer than in CuNi. If that were true, it would open the possibility to observe an unusual type of proximity effect in which spin-triplet pair correlations penetrate deep into the F metal, a situation predicted to occur in S/F systems in the presence of certain forms of magnetic inhomogeneity.<sup>8</sup> Clearly, direct measurements of the spin memory length in PdNi and other ferromagnetic alloys will not only help in the interpretation of existing data on S/F systems, but may also indicate which materials are most likely to be fruitful in future experiments searching for the predicted triplet correlations.<sup>8</sup>

The spin memory length,  $l_{sf}$ , also plays an important role in the context of giant magnetoresistance (GMR) of metallic multilayers.<sup>9</sup> For example, spin memory loss in the nonmagnetic spacer layer (N) in an F/N/F spin valve reduces the GMR signal, whereas spin memory loss

strategically placed in layers outside the active F/N/F core can actually enhance the GMR signal.<sup>10</sup> In ferromagnetic materials, spin memory loss tends to limit the thickness of the F layer that actively contributes to the GMR signal.<sup>11</sup> Measurements of  $l_{sf}$  have been performed on a wide variety of N materials and on a handful of F materials.<sup>12</sup> In this paper, we present measurements of the spin memory length in specific PdNi and PdFe alloys, chosen for reasons stated below.

We chose initially to study Pd<sub>1-x</sub>Ni<sub>x</sub> alloy with  $x = 12$  atomic %, because alloys with concentrations close to that value have been used previously in several studies of S/F systems.<sup>4,7,13,14</sup> The PdNi sputtering target consists of a 5.6-cm diameter target of pure Pd with several 6-mm diameter Ni plugs inserted into the target. The composition of the sputtered material was determined to be  $12.0 \pm 0.5\%$  by energy dispersive X-ray spectroscopy. The Curie temperature of thick films was measured to be 175 K, which is consistent with this composition from earlier measurements.<sup>15</sup> The polycrystalline PdNi films have the expected FCC crystal structure and grow with (111) texture, as determined by X-ray diffraction from a 200-nm thick film. Similar multilayers of other FCC metals grown on thick Nb base layers exhibit columnar growth, with columnar grains of width 20 – 90 nm.<sup>16</sup>

To measure  $l_{sf}$  in the PdNi alloy, we sputtered hybrid spin valves of the form Cu(10)/Py(24)/Cu(20)/PdNi( $d_{PdNi}$ )/Cu(10), where all thickness are specified in nm. In these samples PdNi acts as the “pinned” F layer and permalloy (Py = Ni<sub>84</sub>Fe<sub>16</sub>) as the “free” F layer. Because the coercive field of PdNi ( $H_c \approx 1.5$  kOe, see inset to Fig. 1) is much larger than that of Py ( $H_c < 15$  Oe), we initially believed that exchange bias was not necessary to achieve good antiparallel (AP) alignment of the PdNi and Py magnetizations. (This issue will be discussed further

below.) With the current direction perpendicular to the planes (CPP), the specific resistance is defined as  $AR$  (sample cross-sectional area times CPP resistance), and the specific magnetoresistance is  $A\Delta R = A(R^{AP} - R^P)$ . The sample is sandwiched between two  $\sim 1$ -mm-wide superconducting Nb cross strips, giving  $A \sim 1 \text{ mm}^2$ , and measured at 4.2 K using SQUID electronics in a current comparator bridge. Our sputtering system and measurement electronics are described in detail elsewhere.<sup>17</sup>

A qualitative understanding of the magnetoresistance in our spin valves can be gained from the simple two-current series-resistor model.<sup>18</sup> The model treats transport of up- and down-spin electrons in parallel through the multilayer. In the F materials and at F/N interfaces, the majority and minority spins generally have different resistivities and interface resistances, defined below. When the thickness of the PdNi layer  $d_{PdNi}$  is much less than  $l_{sf}^{PdNi}$ , the two-current series-resistor model<sup>18</sup> gives

$$A\Delta R \propto \beta_{PdNi} \rho_{PdNi}^* d_{PdNi} + \gamma_{PdNi/Cu} AR_{PdNi/Cu}^* \quad (1)$$

When  $d_{PdNi} \gg l_{sf}^{PdNi}$ ,

$$A\Delta R \propto \beta_{PdNi} \rho_{PdNi}^* l_{sf}^{PdNi} + \gamma_{PdNi/Cu} AR_{PdNi/Cu}^* \quad (2)$$

Thus, a plot of  $A\Delta R$  vs.  $d_{PdNi}$  will be linear at small values of the PdNi thickness and saturate at large values. Valet-Fert<sup>9</sup> theory interpolates between these two limiting cases, and the crossover between the two behaviors can be used to extract  $l_{sf}^{PdNi}$ . In Eqs. (1) and (2),  $\beta_{PdNi} = (\rho_{PdNi}^\downarrow - \rho_{PdNi}^\uparrow) / (\rho_{PdNi}^\downarrow + \rho_{PdNi}^\uparrow)$  is the bulk spin-scattering asymmetry, where  $\rho_{PdNi}^{\uparrow(\downarrow)}$  is the resistivity of the PdNi for electrons with their moment parallel (antiparallel) to the moment of the PdNi layer;  $\rho_{PdNi}^* = \rho_{PdNi} / (1 - \beta_{PdNi}^2)$ , and  $\rho_{PdNi} = (1/\rho_{PdNi}^\uparrow + 1/\rho_{PdNi}^\downarrow)^{-1}$  is the usual resistivity of a thick PdNi film.  $AR_{PdNi/Cu}^*$  and the spin scattering asymmetry at the PdNi/Cu interface,  $\gamma_{PdNi/Cu}$ , have similar definitions in terms of  $AR_{PdNi/Cu}^\uparrow$  and  $AR_{PdNi/Cu}^\downarrow$ , where  $AR_{PdNi/Cu}$  is the specific resistance of the PdNi/Cu interface.

Fig. 1 shows the raw magnetoresistance signal for a sample with  $d_{PdNi} = 12 \text{ nm}$ . The sample, immersed in liquid helium, was first subjected to an applied field  $H = -5 \text{ kOe}$  to align the PdNi magnetization ( $M_{PdNi}$ ) in the negative direction. The field was then set to zero, and the sample was slowly lifted in the cryostat to just above the liquid helium level until a NbTi wire mounted near the sample transformed into the normal state. Then the sample was lowered back into the liquid helium. This process removes any trapped magnetic flux from the Nb contacts. Various tests indicate that  $M_{PdNi}$  is not affected by this warming. Once the sample was cold again, the magnetic field was slowly swept from  $H = -500 \text{ Oe}$  to  $H = 500 \text{ Oe}$ , then back to  $H = -500 \text{ Oe}$ . The magnetization of the Py layer switches abruptly when the field passes through zero, indicating that its coercive field is

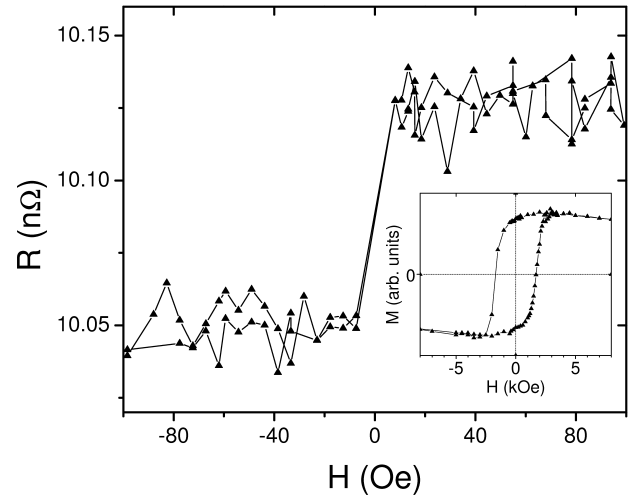


FIG. 1:  $AR$  vs.  $H$  data at 4.2 K for a Py/Cu/PdNi hybrid spin valve with  $d_{PdNi} = 12 \text{ nm}$ . Before taking these data, the PdNi layer was magnetized in the negative direction by applying a magnetic field of  $-5 \text{ kOe}$ . The Py layer switches when the applied field is changed from  $-7.5$  to  $+7.5 \text{ Oe}$ . The inset shows the hysteresis loop at 10 K for a  $[\text{PdNi}(20)/\text{Cu}(10)]_n$  multilayer with  $n = 3$ , where at saturation  $M_{PdNi} = 116 \text{ emu/cm}^3$ . The coercive field is about  $1.5 \text{ kOe}$ , much larger than the fields used to switch the Py layer.

less than the field step size of  $7.5 \text{ Oe}$ . (The figure shows only the region between  $-100$  and  $100 \text{ Oe}$  for clarity.) The reproducibility of the data in the two sweep directions indicates that  $M_{PdNi}$  does not change significantly during the sweep, due to the high coercivity of PdNi shown in the inset.

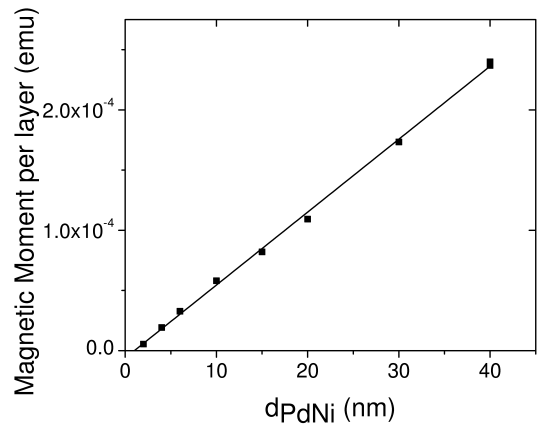


FIG. 2: Magnetic moment per layer of a series of PdNi/Cu multilayers vs. PdNi thickness, at 10 K. The solid line is a best fit straight line, whose x-axis intercept provides an estimate of the total thickness of the magnetically dead layers at the two PdNi/Cu interfaces.

An important issue in the magnetic behavior of

thin films is the possible existence of a magnetic “dead” layer at the interface with a nonmagnetic film, due to the reduced number of magnetic atom nearest neighbors at the interface or to interdiffusion or alloying near the interface. To address this, we grew a series of PdNi multilayers of the form Nb(5)/Cu(10)/[PdNi( $d_{PdNi}$ )/Cu(10)] $_n$ /Nb(5), where  $d_{PdNi}$  varied between 2 and 40 nm, and  $n$  was chosen to keep the total PdNi thickness equal to 60 nm (except  $n = 1$  for  $d_{PdNi} = 40$  nm). The inset to Fig. 1 shows the magnetization vs. field for the sample with  $d_{PdNi} = 20$  nm, measured at  $T = 10$  K in a Quantum Design SQUID magnetometer, where we have not subtracted out the small diamagnetic contribution from the substrate, visible at high field. Fig. 2 shows the magnetic moment per layer (at saturation) vs.  $d_{PdNi}$  for all the multilayer samples. A linear fit extrapolates to zero at  $d_{PdNi} = 1.1 \pm 0.4$  nm, which we interpret as the total thickness of the dead layers ( $\delta_{dead}$ ) at the two PdNi/Cu interfaces.

Fig. 3 shows the specific magnetoresistance,  $A\Delta R$ , vs. PdNi thickness, for all of our samples. The data start out increasing nearly linearly with  $d_{PdNi}$ , then flatten out when  $d_{PdNi}$  exceeds about 10 nm. The solid line is a fit to the data of the Valet-Fert equations.<sup>9</sup> Many of the material parameters used in the fit are obtained from previous measurements. These include the resistivity and bulk spin scattering asymmetry for Py,  $\rho_{Py} = 123$  n $\Omega$ m and  $\beta_{Py} = 0.76$ ,<sup>19</sup> the specific resistance and spin scattering asymmetry for the inner Py/Cu interface,  $AR_{Py/Cu}^* = 0.50$  f $\Omega$ m<sup>2</sup> and  $\gamma_{Py/Cu} = 0.70$ , and the spin memory length in Py,  $l_{sf}^{Py} = 5.5$  nm.<sup>19</sup> For the Cu layer between the Py and PdNi layers, we take  $\rho_{Cu} = 4.5$  n $\Omega$ m<sup>19</sup> and  $l_{sf}^{Cu} \geq 500$  nm.<sup>12</sup> We estimate the resistivity of PdNi alloy from Van der Pauw measurements on isolated films of thickness 200 nm that give  $\rho_{PdNi} = 121 \pm 6$  n $\Omega$ m. The interface resistance between PdNi and Cu and the extent of spin memory loss at the PdNi/Cu interface are estimated from earlier work on the Pd/Cu interface,<sup>20</sup> which gave  $AR_{Pd/Cu}^* = 0.42 \pm 0.07$  f $\Omega$ m<sup>2</sup> and  $\delta_{Pd/Cu} = 0.24_{-0.03}^{+0.06}$ , where the spin polarization passing through the interface is reduced by the factor  $e^{-\delta}$ . For simplicity, we assume no spin scattering asymmetry at the inner PdNi/Cu interface, i.e.  $\gamma_{PdNi/Cu} = 0$ . The free parameters in the fit are then  $\beta_{PdNi}$ ,  $AR_{PdNi/Cu/Nb}$ ,<sup>21</sup> and the quantity we are most interested in, namely  $l_{sf}^{PdNi}$ , the spin memory length in our PdNi alloy.

To further constrain the fitting parameters, we also fit the total resistance of the spin valve in the antiparallel state,  $AR^{AP}$ , shown in Fig. 4. For this, we need the interface resistance between the Py and Nb layers (separated by the Cu spacer, which is superconducting by proximity), known to be  $AR_{Py/Cu/Nb} = 3.0$  f $\Omega$ m<sup>2</sup>.<sup>19,21</sup>

In the numerical solution of the Valet-Fert equations, we include a magnetically dead layer at the PdNi/Cu interfaces with total thickness  $\delta_{dead}$ , following the discussion earlier. The best fit to the data, shown as

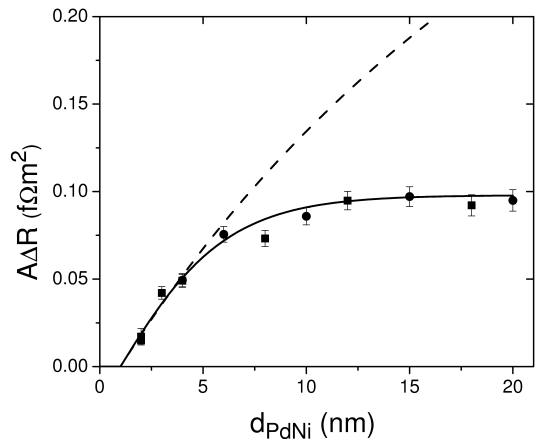


FIG. 3:  $A\Delta R$  vs.  $d_{PdNi}$ . The solid line represents a fit to the data of the Valet-Fert equations, using fixed parameters discussed in the text. The fit provides an estimate of the spin memory length in PdNi of  $l_{sf}^{PdNi} = 2.8 \pm 0.5$  nm. The dashed line shows the result of a calculation assuming  $l_{sf}^{PdNi} = \infty$ .

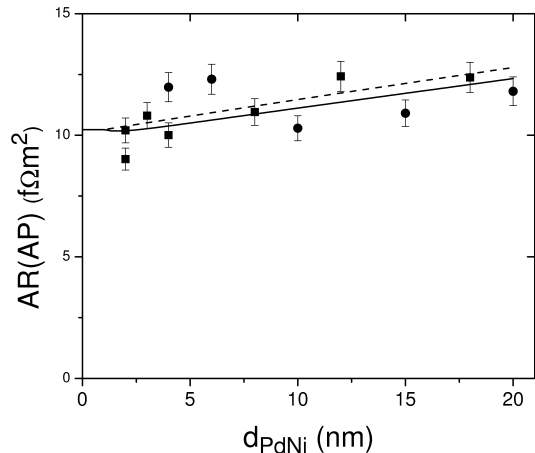


FIG. 4:  $AR$  vs.  $d_{PdNi}$  for the AP state. The solid line is the result of a calculation with the same parameters used to fit the data in Fig. 3. The dashed line is for  $l_{sf}^{PdNi} = \infty$ .

the solid lines in Figs. 3 and 4, is obtained with  $\delta_{dead} = 1.0 \pm 0.2$  nm, a bulk spin-scattering asymmetry of  $\beta_{PdNi} = 0.14 \pm 0.02$ , a spin memory length in PdNi of  $l_{sf}^{PdNi} = 2.8 \pm 0.5$  nm and a PdNi/Nb interface resistance of  $AR_{PdNi/Cu/Nb} = 2.3 \pm 0.3$  f $\Omega$ m<sup>2</sup>. These uncertainties are based on the scatter in the data and the uncertainty in  $\rho_{PdNi}$ . To illustrate the role of the finite spin memory length in the fit, we show with the dashed line in Fig. 3 the result of the calculation taking  $l_{sf}^{PdNi} = \infty$ . The value obtained for the PdNi/Nb interface resistance is consistent with the value  $AR_{PdNi/Nb} = 2.31 \pm 0.07$  f $\Omega$ m<sup>2</sup> obtained from the high-bias resistance of Josephson junctions of the form Nb/PdNi/Nb, with PdNi thicknesses in the range 30-100 nm.<sup>22</sup>

In Fig. 4, the dashed line, for  $l_{sf}^{PdNi} = \infty$ , is not much different from the solid line for  $l_{sf}^{PdNi} = 2.8$ . Thus the fit to these  $AR$  data is not very sensitive to the choice of  $l_{sf}^{PdNi}$ . The slope of the solid line agrees reasonably well with data, indicating that our value of  $\rho_{PdNi}$  from van der Pauw measurements on 200-nm-thick films is consistent with these CPP results. The value of  $AR_{PdNi/Cu/Nb}$  is determined primarily from this fit in Fig. 4, and its value has only a minor effect on the fit to the  $A\Delta R$  data of Fig. 3.

The very short value of  $l_{sf}^{PdNi}$  obtained from these measurements was at first a surprise, because it is much shorter than the decay length of the supercurrent in Nb/PdNi/Nb Josephson junctions reported recently by some of us.<sup>22</sup> Theoretical analysis of the Josephson junction data suggests that the decay length should be equal to the mean free path in PdNi, which was determined to be  $l_e = 10.6 \pm 1$  nm from a fit to the critical current data.<sup>23</sup> In the standard picture of diffusive transport in metals, spin-flip and spin-orbit scattering occur on length scales much longer than the mean free path. The data from these two experiments, however, indicate the opposite behavior for our PdNi films, namely  $l_{sf} < l_e$ . A possible explanation for this unusual situation comes from our recent discovery that the magnetic anisotropy in our thin PdNi films is out-of-plane.<sup>22</sup> That discovery casts doubt on our ability to produce a good AP state in our spin valve samples. Indeed, the  $M$  vs.  $H$  data shown in the inset to Fig. 1 are slightly rounded, with the remanent magnetization equal to about 80% of the saturation magnetization. We now know that this rounding is due to the PdNi magnetization starting to rotate out of the plane, because similar  $M$  vs  $H$  curves taken with  $H$  pointing out of the plane are less rounded (see Fig. 3 of ref. [22]). The out-of-plane component of the PdNi magnetization can cause rotation of spins initially aligned along the in-plane Py magnetization direction, enhancing spin memory loss in our spin valves.

To suppress the influence of the out-of-plane magnetic anisotropy on our spin valve results, we have fabricated a second set of spin valve samples of the form Cu(10)/Py(24)/Cu(20)/PdNi( $d_{PdNi}$ )/Py(8)/FeMn(8)/Cu(10), with  $d_{PdNi}$  ranging from 0 to 20 nm. In these samples, the PdNi is exchange coupled to the thin Py layer, which is in turn exchange biased in-plane by the FeMn.<sup>24</sup> After fabrication, these samples are heated to 170 C (above the blocking temperature of FeMn), then cooled to room temperature in an in-plane field of 190 Oe. Magnetization measurements on PdNi/Py/FeMn test samples show that both the Py and PdNi are exchange biased by this procedure. Thus the in-plane Py magnetization constrains the PdNi magnetization to also stay in-plane. In these spin valves, the PdNi acts as a "spoiler" layer<sup>25</sup> inserted into a high-performance Py/Cu/Py spin valve, because  $\beta_{PdNi} \ll \beta_{Py}$ . When the PdNi layer is thin, the GMR signal is large, whereas as the PdNi layer gets thicker, the signal diminishes until it finally reaches a much smaller value corresponding

to that of a Py/Cu/PdNi spin valve. The Valet-Fert equations describe this process quantitatively as  $d_{PdNi}$  surpasses  $l_{sf}^{PdNi}$ .

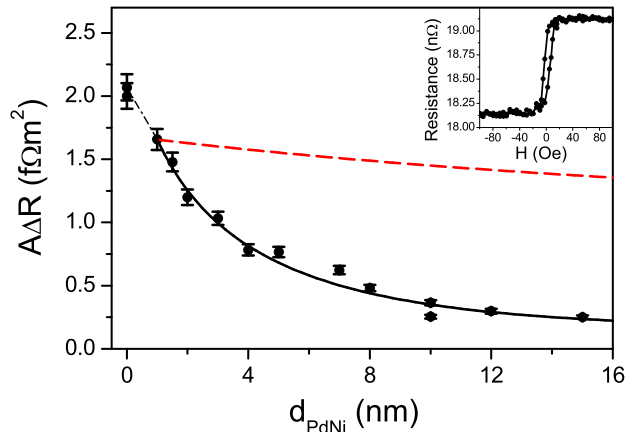


FIG. 5:  $A\Delta R$  vs.  $d_{PdNi}$  for "spoiler" spin valves of the form Py/Cu/PdNi/Py/FeMn. Without PdNi, these are high-performance Py/Py spin valves with large  $A\Delta R$ . As the PdNi thickness increases,  $A\Delta R$  drops because of the low spin-scattering asymmetry in PdNi relative to Py, i.e.  $\beta_{PdNi} \ll \beta_{Py}$ . The black dot-dashed line shows a linear interpolation between first two points. The black solid line is a fit to the Valet-Fert equations for the rest of the points, giving  $l_{sf}^{PdNi} = 5.4 \pm 0.6$  nm. The red large-dashed line is obtained with  $l_{sf}^{PdNi} = \infty$ . Inset: Raw magnetoresistance data for the sample with  $d_{PdNi} = 2$  nm.

Fig. 5 shows  $A\Delta R$  vs. PdNi thickness for the "spoiler" samples. (Raw GMR data for the sample with  $d_{PdNi} = 2$  nm are shown in the inset.) As expected,  $A\Delta R$  starts at a large value, and decreases with increasing PdNi thickness. To extract  $l_{sf}^{PdNi}$  from these data, we again perform a numerical evaluation of the Valet-Fert equations. The data points at  $d_{PdNi} = 0$  are treated separately, since those two samples (from separate sputtering runs) contain neither a PdNi/Cu nor a PdNi/Py interface. For the rest of the data points starting at  $d_{PdNi} = 1.0$  nm, we assume a magnetically 0.5-nm thick dead layer at the PdNi/Cu interface following the earlier discussion, and, for simplicity, a 0.5-nm-thick PdNi/Py interface. We obtain a constraint between the interface parameters,  $\gamma_{PdNi/Py}$  and  $AR_{PdNi/Py}^*$ , by requiring the calculation to agree with the  $A\Delta R$  datum point at  $d_{PdNi} = 1$  nm. The overall  $\chi^2$  is relatively insensitive to the exact choice of  $\gamma_{PdNi/Py}$  and  $AR_{PdNi/Py}^*$  within the constraint; fortunately, however, the best-fit value of  $l_{sf}^{PdNi}$  changes little across the range of those interface parameters. The fit leads us to the values  $\gamma_{PdNi/Py} = 0.70 \pm 0.25$  and  $AR_{PdNi/Py}^* = 1.3 \mp 0.9$  f $\Omega m^2$ , rather different from the Py/Pd interface parameters of  $\gamma_{Pd/Py} = 0.41 \pm 0.14$  and  $AR_{Pd/Py}^* = 0.2 \pm 0.1$  f $\Omega m^2$ .<sup>26</sup> It appears that the presence of Ni in the Pd significantly enhances the PdNi/Py interface parameters, even though  $\beta_{PdNi}$  is very small. Using

the parameters already applied to the fit in Fig. 3, with the exception of  $l_{sf}^{PdNi}$ , we obtain  $l_{sf}^{PdNi} = 5.4 \pm 0.6$  nm for this "spoiler" spin valve.

The longer value of  $l_{sf}^{PdNi}$  obtained from the second set of experiments supports the hypothesis that the PdNi magnetization is highly non-uniform in the first set of spin valves with the stand-alone PdNi fixed layer. Electrons moving through the PdNi experience an inhomogeneous exchange field, resulting in rapid spin memory loss. This process may not be accompanied by efficient momentum scattering, hence it allows the possibility of realizing the regime  $l_{sf} < l_e$ . The fact that we obtain  $l_{sf} < l_e$  also for the second set of samples seems to indicate the presence of non-uniform magnetization even when the PdNi layer is exchange-coupled to the adjacent Py layer with in-plane magnetization, although the effect is smaller than in the first set of samples.

What is the origin of the out-of-plane magnetic anisotropy in PdNi films? While carrying out these experiments, we learned of work by Campbell and co-workers 30 years ago demonstrating that Ni impurities in Pd exhibit a strong orbital magnetic moment, which is indicative of strong spin-orbit coupling.<sup>27,28</sup> If the PdNi films grow with uniform strain in the plane, the spin-orbit coupling may induce out-of-plane magnetic anisotropy. (This depends on whether the strain is tensile or compressive in the plane, and the sign of the spin-orbit coupling constant.) Furthermore, local inhomogeneities in the strain due to crystalline defects or grain boundaries could produce local fluctuations in the magnetic anisotropy direction, which enhances spin memory loss as described above. A surprising aspect of this story is the relatively long decay length, 10.6 nm, of the critical current in Nb/PdNi/Nb Josephson junctions.<sup>22,23</sup> If our hypothesis describing the local inhomogeneous magnetization in PdNi is correct, then it appears that the Cooper pairs are not as sensitive to magnetic disorder as is the single-electron spin memory length. This is plausible given that the two spins in the Cooper pair both precess in the same direction around the local exchange field, maintaining their spin-singlet state in spite of the rapidly changing exchange field. Confirmation or refutation of this picture will require a real theoretical calculation.

The measurements by Campbell and co-workers in the 1970's, in addition to implicating strong spin-orbit coupling in PdNi alloy, also showed that spin-orbit coupling in dilute PdFe alloys is comparatively weak. In fact, a later study<sup>29</sup> of the ac susceptibility of  $Pd_{1-x}Fe_x$  alloys described the alloy with  $x = 1.4\%$  as "a nearly ideal system," in the sense that the critical exponents at the Curie temperature follow predictions of the Heisenberg model, and the magnetocrystalline anisotropy is very small. These observations motivated us to measure  $l_{sf}$  in PdFe, with the hope that it would be much longer than in PdNi.

PdFe films were sputtered using a 5.6-cm diameter Pd target with a single Fe plug of diameter 6.6

mm in the center. Our magnetization measurements on PdFe films support the idea of low magnetocrystalline anisotropy. Fig. 6 shows  $M$  vs.  $H$  data at  $T = 10$  K for a 80 nm thick PdFe film grown in the form Nb(150)/Cu(10)/PdFe(80)/Cu(10)/Nb(25), with  $H$  both in-plane and out-of-plane. Relatively sharp switching to the saturation magnetization is observed for  $H$  in-plane, whereas for  $H$  out-of-plane saturation isn't achieved until  $H$  exceeds the demagnetizing field of  $\approx 300$  Oe. The strong preference for in-plane magnetization indicates dominance of shape anisotropy over magnetocrystalline anisotropy in these PdFe thin films. Similar indications of in-plane anisotropy were also seen in a 60 nm thick film of similar structure to the 80 nm film and in a stand-alone 400 nm thick PdFe film (data not shown). The temperature dependence of the magnetization for the 80 and 400 nm PdFe films is shown in Fig. 7. The 80 nm film showed smaller magnetization and Curie temperature compared to the 400 nm film, which could be due to strain during growth. The Curie temperature of 44 K obtained from the 400 nm thick film provides an estimate of the Fe concentration of 1.1 atomic %.<sup>29</sup> A direct measurement of the Fe concentration by energy dispersive X-ray spectroscopy on the same sample yielded a somewhat larger result, 1.6 at. %, but with a large uncertainty due to the very small Fe concentration. The in-plane saturation magnetization of PdFe measured on the 400 nm film at 10 K was  $M_{PdNi} = 63 \text{ emu/cm}^3 = 0.1 \mu_B/\text{Fe atom}$ , which according to ref. 29 corresponds to an Fe concentration of approximately 1.4 at. %. These three determinations of the Fe concentration are reasonably consistent, and lead us to our best estimate of 1.3 at. %.

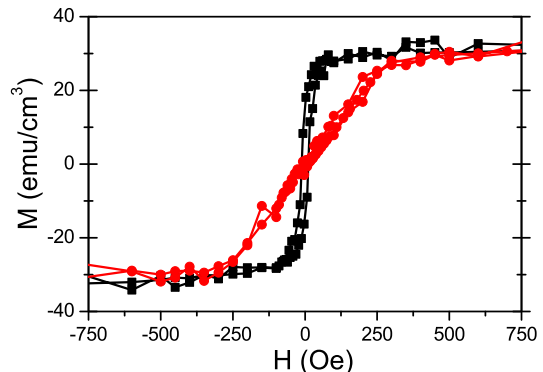


FIG. 6: (Color online)  $M$  vs.  $H$  at  $T=10$  K for a 80 nm thick PdFe film grown in a Nb(150)/Cu(10)/PdFe(80)/Cu(10)/Nb(25) multilayer, with  $H$  pointing in-plane (black squares) and out-of-plane (red circles).

To measure  $l_{sf}$  of PdFe, we sputtered hybrid spin valves of the form Cu(5)/FeMn(8)/Py(8)/Cu(10)/PdFe( $d_{PdFe}$ )/Cu(10)/Py(8)/FeMn(8)/Cu(5), again sandwiched between thick

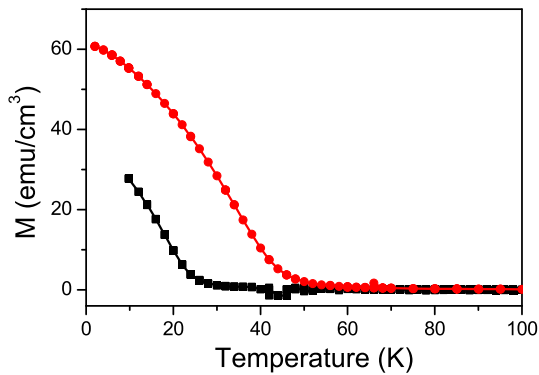


FIG. 7: (Color online)  $M$  vs.  $T$  for PdFe films of thickness 80 nm (black squares) and 400 nm (red circles). The films were zero-field cooled to low temperature and then the magnetization was measured by applying an in-plane field of 500 G. The temperature was then increased gradually to 100 K keeping the field constant. The Curie temperature of the 400 nm film indicated an Fe concentration of about 1.1%.

Nb electrodes. The finished samples are heated to 170 C and cooled in a field of 190 Oe to pin the two Py layers to the FeMn via exchange bias. These samples can be thought of as two FeMn/Py/Cu/PdFe hybrid spin valves back-to-back, with their magnetoresistance signals adding. The advantages of this geometry relative to the first geometry we used with PdNi are that the magnetoresistance signal is twice as large, and there are no interfaces between PdFe and Nb, hence there are fewer parameters to take from previous work.

Raw magnetoresistance data are shown in the inset to Fig. 8 for the sample with  $d_{PdFe} = 15$  nm. As expected, the PdFe layer switches its magnetization at a small field. A plot of  $A\Delta R$  vs.  $d_{PdFe}$  is shown in Fig. 8, along with a fit to the Valet-Fert equations. For this fit, the value of  $\rho_{PdFe}$  is needed. From separate measurements on 100- and 200-nm-thick PdFe films, we have  $\rho_{PdFe} = 85 \pm 4$  n $\Omega$ m. For the PdFe/Cu interfaces, we use the same parameters as with PdNi/Cu. Fig. 8 shows the fit assuming that  $\delta_{dead} = 0$  for the PdFe/Cu interfaces. If  $\delta_{dead} = 1$  nm, as assumed for the PdNi/Cu interfaces, the fit in Fig. 8 is slightly changed at small  $d_{PdFe}$ . Including the effect of these two choices of  $\delta_{dead}$  on the fits, we obtain  $\beta_{PdFe} = 0.11 \pm 0.02$  and  $l_{sf}^{PdFe} = 9.6 \pm 2$  nm.

It is instructive to ask whether the values of the spin memory lengths obtained in this work can be estimated from a previous measurement of the spin memory length in nominally pure Pd,<sup>30</sup> combined with the assumption that the spin memory length is proportional to the mean free path, hence inversely proportional to the resistivity.<sup>12</sup> The previous measurements on sputtered Pd gave  $\rho_{Pd} = 42 \pm 2$  n $\Omega$ m and  $l_{sf}^{Pd} = 25^{+10}_{-5}$  nm.<sup>30</sup> With these values, we expect  $l_{sf}^{PdFe} \approx l_{sf}^{Pd} * (\rho_{Pd} / \rho_{PdFe}) \approx 12^{+5}_{-2.6}$  nm, and  $l_{sf}^{PdNi} \approx l_{sf}^{Pd} * (\rho_{Pd} / \rho_{PdNi}) \approx 8.7^{+3.5}_{-1.8}$  nm. The former overlaps our measured value of  $l_{sf}^{PdFe} = 9.6 \pm 2$  nm,

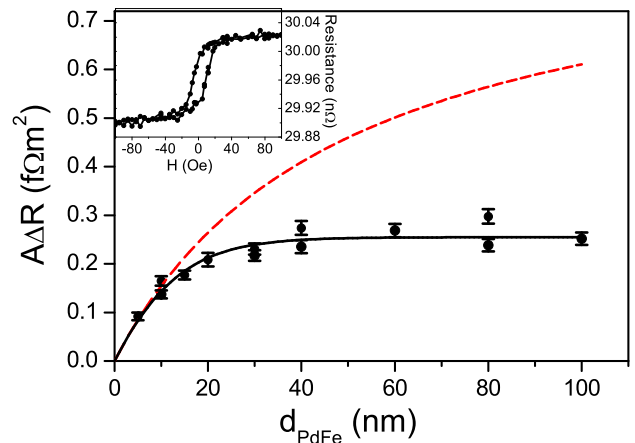


FIG. 8:  $A\Delta R$  vs.  $d_{PdFe}$  for the double hybrid spin valves containing Py and PdFe alloy. The black solid line is a fit to the data of the Valet-Fert equations, with the spin memory length in PdFe of  $l_{sf}^{PdFe} = 9.6 \pm 2.0$  nm. The red dashed line shows the result of a calculation assuming  $l_{sf}^{PdFe} = \infty$ . Inset: Raw magnetoresistance data for the sample with  $d_{PdFe} = 15$  nm.

whereas the latter is still a bit larger than our measured value of  $l_{sf}^{PdNi} = 5.4 \pm 0.6$  nm. Perhaps this disagreement is due to the stronger spin-orbit scattering in PdNi.<sup>27,28</sup> It is unfortunate that the mean free path in Pd and its alloys is difficult to determine independently.<sup>22</sup> Indeed, if it is true that  $l_{sf}^{PdNi} < l_e^{PdNi}$ , as discussed earlier, then the whole argument leading to the relationship above might be invalid.

In conclusion, we have measured the spin memory length in Pd<sub>0.88</sub>Ni<sub>0.12</sub> and Pd<sub>0.987</sub>Fe<sub>0.013</sub> alloys using giant magnetoresistance methods. For PdNi, two different methods were used, resulting in the values  $l_{sf}^{PdNi} = 2.8 \pm 0.5$  nm and  $5.4 \pm 0.6$  nm. We believe that the smaller of these values results from a conflict between the in-plane quantization axis imposed by the experimental geometry and data analysis and the recently-discovered out-of-plane magnetic anisotropy in PdNi films. This conflict produces inhomogeneous magnetization in the samples, which in turn results in severe spin memory loss. The effect is mitigated somewhat when the PdNi magnetization is pinned by an adjacent Py layer. In PdFe, we find  $l_{sf}^{PdFe} = 9.6 \pm 2$  nm, a considerably larger value than in PdNi.

In closing, we note that the spin memory lengths measured in these Pd alloys are considerably longer than what is found in another popular weakly ferromagnetic alloy, CuNi.<sup>5,6</sup> If one wants to use one of these alloys in a search for superconducting correlations with spin-triplet symmetry,<sup>8</sup> however, one must beware of their limitations. The cleanest signature of the so-called “long-range triplet correlations” would be observation of a proximity or Josephson effect penetrating a ferromagnet over a distance much longer than the length scale associated

with conventional spin-singlet correlations. The latter scale is usually the larger of the mean free path,  $l_e$ , or the dirty-limit exchange length,  $\xi_F = \sqrt{(\hbar D/E_{ex})}$ . As discussed earlier in this paper, it appears that  $l_{sf}^{PdNi}$  is shorter than  $l_e^{PdNi}$ , eliminating any hope of observing long-range triplet correlations in PdNi alloy. In PdFe the situation is slightly better, but still not ideal, as we

expect the mean free path of the 1.4% Fe alloy to be longer than that of the 12% Ni alloy.

Acknowledgments: We thank I.A. Campbell for bringing references [27,28] to our attention and for helpful discussions, and B. Bi for performing X-ray scattering measurements on our PdNi films. This work was supported by the US-DOE under grant DE-FG02-06ER46341.

- 
- \* Electronic address: birge@pa.msu.edu
- <sup>1</sup> P.G. DeGennes, Phys. Lett. **23**, 10 (1966).
  - <sup>2</sup> A.I. Buzdin, Rev. Mod. Phys. **77**, 935 (2005), and references therein.
  - <sup>3</sup> V.V. Ryazanov, V.A. Oboznov, A.Yu. Rusanov, A.V. Veretennikov, A.A. Golubov, and J. Aarts, Phys. Rev. Lett. **86**, 2427 (2001).
  - <sup>4</sup> T. Kontos, M. Aprili, J. Lesueur, and X. Grison, Phys. Rev. Lett. **86**, 304 (2001).
  - <sup>5</sup> V. A. Oboznov, V. V. Bol'ginov, A. K. Feofanov, V. V. Ryazanov, and A.I. Buzdin, Phys. Rev. Lett. **96**, 197003 (2006).
  - <sup>6</sup> B. Baker, R. Loloee and W.P. Pratt, Jr. (unpublished).
  - <sup>7</sup> T. Kontos, M. Aprili, J. Lesueur, F. Genet, B. Stephanidis, and R. Boursier, Phys. Rev. Lett. **89**, 137007 (2002).
  - <sup>8</sup> A. F. Volkov, F. S. Bergeret, and K. B. Efetov, Phys. Rev. Lett. **90**, 117006 (2003).
  - <sup>9</sup> T. Valet, and A. Fert, Phys. Rev. B **48**, 7099 (1993).
  - <sup>10</sup> S. Urazhdin, N.O. Birge, W.P. Pratt, Jr., and J. Bass, J. Appl. Phys. **84**, 1516 (2004).
  - <sup>11</sup> See section 2.2.2.(b1) of ref. [12].
  - <sup>12</sup> J. Bass and W. P. Pratt Jr., J. Phys. Condens. Matter **19** 183201 (2007).
  - <sup>13</sup> C. Cirillo, J. Aarts, and C. Attanasio, Phys. Stat. Sol. **3**, 3015 (2006).
  - <sup>14</sup> K. Matsuda, H. Niwa, Y. Akimoto, T. Uemura, and M. Yamamoto, IEEE Trans. Appl. Supercond. **17**, 3529 (2007).
  - <sup>15</sup> T. Kontos, Ph.D. thesis, Université Paris XI, Orsay (2002).
  - <sup>16</sup> H. Geng, J.W. Heckman, W.P. Pratt, J. Bass, F.J. Espinosa, S.D. Conradson, D. Lederman, and M.A. Crimp, J. Appl. Phys. **86** 4166 (1999).
  - <sup>17</sup> S. F. Lee, Q. Yang, P. Holody, R. Loloee, J. H. Hetherington, S. Mahmood, B. Ikegami, K. Vigen, L. L. Henry, P. A. Schroeder, W. P. Pratt Jr., and J. Bass, Phys. Rev. B **52**, 15426 (1995).
  - <sup>18</sup> J. Bass and W. P. Pratt Jr., J. Magn. Magn. Mater. **200**, 274 (1999), and references therein.
  - <sup>19</sup> L. Vila, W. Park, J.A. Caballero, D. Bozec, R. Loloee, W. P. Pratt Jr., and J. Bass, J. Appl. Phys. **87**, 8610 (2000), and references therein.
  - <sup>20</sup> C. Galinon, K. Tewolde, R. Loloee, W.-C. Chiang, S. Olson, H. Kurt, W. P. Pratt Jr., J. Bass, P.X. Xu, Ke Xia, and M. Talanana, Appl. Phys. Lett. **86**, 182502 (2005).
  - <sup>21</sup> Concerning the outer PdNi/Cu and Py/Cu interfaces, prior work indicates that the interface spin scattering asymmetry,  $\gamma_{F/Cu}$ , is suppressed at any F/Cu/Nb interface due to Andreev reflection, where F = PdNi or Py for this work. See K. Eid, H. Kurt, W.P. Pratt, Jr., and J. Bass, Phys. Rev. B **70**, 100411(R) (2004). For the present work,  $\gamma_{Py/Cu}$  is irrelevant at the outer Py/Cu interface for the additional reason that  $d_{Py} \gg l_{sf}^{Py}$ .
  - <sup>22</sup> T.S. Khaire, W.P. Pratt, Jr., and N.O. Birge, Phys. Rev. B **79**, 094523 (2009).
  - <sup>23</sup> The critical current of the Nb/PdNi/Nb Josephson junctions studied in [22] actually decayed exponentially with a decay length of  $7.7 \pm 0.5$  nm. The theoretical formula to describe the decay, however, contains a sum over Matsubara frequencies. The result is that the primary decay constant in the fit, which should be equal to the mean free path, was determined to be  $10.6 \pm 1$  nm.
  - <sup>24</sup> J. Nogués and I.K. Schuller, J. Magn. Magn. Mater. **192**, 203 (1999).
  - <sup>25</sup> C.E. Moreau, I.C. Moraru, N.O. Birge, and W.P. Pratt Jr., Appl. Phys. Lett. **90** 012101 (2007).
  - <sup>26</sup> A. Sharma, J.A. Romero, N. Theodoropoulou, R. Loloee, W.P. Pratt Jr., and J. Bass, J. Appl. Phys. **102**, 113916 (2007).
  - <sup>27</sup> L.D. Khoi, P. Veillet, and I.A. Campbell, J. Phys. F **6** L-197 (1976).
  - <sup>28</sup> S. Senoussi, I.A. Campbell, and A. Fert, Sol. St. Comm. **21** 269 (1977).
  - <sup>29</sup> Z. Wang, H.P. Kunkel, and G. Williams, J. Phys.: Condens. Matter **4** 10385 (1992).
  - <sup>30</sup> H. Kurt, R. Loloee, K. Eid, W.P. Pratt Jr., and J. Bass, Appl. Phys. Lett. **81** 4787 (2002).